nature plants

LETTERS

https://doi.org/10.1038/s41477-021-01015-8

Check for updates

Pluripotency acquisition in the middle cell layer of callus is required for organ regeneration

Ning Zhai[1,2] and Lin Xu[1]✉

In plant tissue culture, callus forms from detached explants in response to a high-auxin-to-low-cytokinin ratio on callus-inducing medium. Callus is a group of pluripotent cells because it can regenerate either roots or shoots in response to a low level of auxin on root-inducing medium or a high-cytokinin-to-low-auxin ratio on shoot-inducing medium, respectively[1]. However, our knowledge of the mechanism of pluripotency acquisition during callus formation is limited. On the basis of analyses at the single-cell level, we show that the tissue structure of *Arabidopsis thaliana* callus on callus-inducing medium is similar to that of the root primordium or root apical meristem, and the middle cell layer with quiescent centre-like transcriptional identity exhibits the ability to regenerate organs. In the middle cell layer, WUSCHEL-RELATED HOMEOBOX5 (WOX5) directly interacts with PLETHORA1 and 2 to promote *TRYPTOPHAN AMINOTRANSFERASE OF ARABIDOPSIS1* expression for endogenous auxin production. WOX5 also interacts with the B-type ARABIDOPSIS RESPONSE REGULATOR12 (ARR12) and represses A-type *ARR*s to break the negative feedback loop in cytokinin signalling. Overall, the promotion of auxin production and the enhancement of cytokinin sensitivity are both required for pluripotency acquisition in the middle cell layer of callus for organ regeneration.

To study cell identities of callus, we performed single-cell RNA sequencing (RNA-seq) using *Arabidopsis* Col-0 hypocotyl explants cultured on callus-inducing medium (CIM) for six days (Supplementary Fig. 1). Ten cell clusters (clusters 0 to 9) were visualized on the basis of the uniform manifold approximation and projection (UMAP)[2] algorithm (Fig. 1a,b and Supplementary Table 1). Clusters 0 to 5 comprised the callus cells, which could be grouped into three cell layers[3]. The outer cell layer (clusters 0 and 1) expressed the epidermis cell markers *3-KETOACYL-COA SYNTHASE6* (*KCS6*)[4], *PROTODERMAL FACTOR1* (*PDF1*)[5], *BODYGUARD* (*BDG*)[6] and *A. thaliana MERISTEM LAYER1* (*ATML1*)[7] (cluster 0), and the lateral root cap marker *PIN-FORMED2* (*PIN2*)[8] (cluster 1) (Fig. 1b). The middle cell layer (cluster 2) had the quiescent centre (QC)-like transcriptional feature co-expressing the marker genes *SCARECROW* (*SCR*)[9], *SCHIZORIZA* (*SCZ*)[10], *JACKDAW* (*JKD*)[11], *PLETHORA1* and *2* (*PLT1/2*; ref. [12]) and *WOX5* (ref. [13]) (Fig. 1b). The index of cell identity (ICI)[14] (Fig. 1c) and AUCell[15,16] (Fig. 1d) analyses showed that the QC-identity gene network was primarily presented by cells from cluster 2. Gene Ontology (GO) analysis showed that the genes related to meristem and auxin were highly enriched in cluster 2 (Fig. 1e and Supplementary Table 2). The inner cell layer (clusters 3 to 5) expressed the vascular initial and provasculature markers *TARGET OF MONOPTEROS5* (*TMO5*)[17], *NAKED PINS IN YUC MUTANTS4* (*NPY4*)[18], *HANABA TARANU* (*HAN*)[19] and *SUPPRESSOR OF MAX2 1-LIKE3* (*SMXL3*)[20] (Fig. 1b). A small portion of cells in clusters 3 and 4 also showed *WOX5* expression (Fig. 1b) and QC-like transcriptional identity (Fig. 1c,d), indicating that there could be transitional cell fate from the middle cell layer to the inner cell layer. Cluster 6 contained vascular cells from the explant and expressed the vasculature markers *AINTEGUMENTA* (*ANT*)[21], *ATHB8* (refs. [21,22]), *PHLOEM INTERCALATED WITH XYLEM* (*PXY*)[21,23], *4-COUMARATE:COA LIGASE1* (*4CL1*)[24], *WALLS ARE THIN1* (*WAT1*)[25] and *bHLH68* (ref. [26]) (Fig. 1b). The callus founder cell marker *WOX11* (ref. [27]) was also specifically expressed in cluster 6, indicating that callus was initiated from cells in cluster 6 (Fig. 1b). Cluster 7 comprised cells in division and expressed the marker genes *HINKEL* (*HIK*)[28] and *TANGLED1* (*TAN1*)[29] (Fig. 1b). The reconstructed trajectory indicated two directions of differentiation from the middle cell layer to the outer and inner cell layers in callus on CIM (Fig. 1f).

We confirmed the expression patterns of *WOX11* in the founder cells from the explant vasculature[27] (Fig. 1g), *ATML1* in the outer cell layer of callus[30] (Fig. 1h) and *WOX5* and *PLT1* in the middle cell layer of callus[3] (Fig. 1i,j and Supplementary Video 1) using the ClearSee assay[31]. After callus was moved to shoot-inducing medium (SIM), *WOX5* expression gradually reduced from the middle cell layer within 48 h (Supplementary Fig. 2). The strong cytokinin response shown by the $TCSn_{pro}$–*mGFP5–ER* reporter line was mainly in the middle and inner cell layers on SIM (Supplementary Fig. 3). The shoot progenitor marker gene *WUS* was induced by cytokinin mainly in the middle cell layer of callus on SIM (Supplementary Fig. 3), indicating that the middle cell layer was capable of fate transition to form shoots. To confirm that shoots regenerate from the middle cell layer expressing *WOX5*, we traced cell lineages using the CRE/LOX system controlled by the *WOX5* promoter[32]. The results showed that the cells forming adventitious shoots were descendants of *WOX5*-expressing cells within the callus (Supplementary Fig. 3). After callus was moved to root-inducing medium (RIM), *WOX5* expression was gradually restricted from the middle cell layer to the stem cell niche during the formation of the root apical meristem (RAM; Supplementary Fig. 2).

We next focused on the role of *WOX5* in the middle cell layer of callus. Our yeast two-hybrid and co-immunoprecipitation (Co-IP) data and a recent study[33] both showed that WOX5 could directly interact with PLT1/2 (Fig. 2a,b). Previous studies indicated that *WOX5* and its redundant homologue *WOX7* as well as *PLT1* and its redundant homologue *PLT2* are required for shoot regeneration from callus[34,35]. We confirmed that *wox5-1 wox7-1* and *plt1-21 plt2-21* exhibited significantly reduced shooting ability on SIM (Fig. 2c and Supplementary Fig. 1) and rooting ability on RIM (Fig. 2d and Supplementary Fig. 1), compared with Col-0. We identified 21 genes that were both downregulated in calli from *wox5-1 wox7-1* and

[1]National Key Laboratory of Plant Molecular Genetics, CAS Center for Excellence in Molecular Plant Sciences, Institute of Plant Physiology and Ecology, Chinese Academy of Sciences, Shanghai, China. [2]University of Chinese Academy of Sciences, Beijing, China. ✉e-mail: xulin@cemps.ac.cn

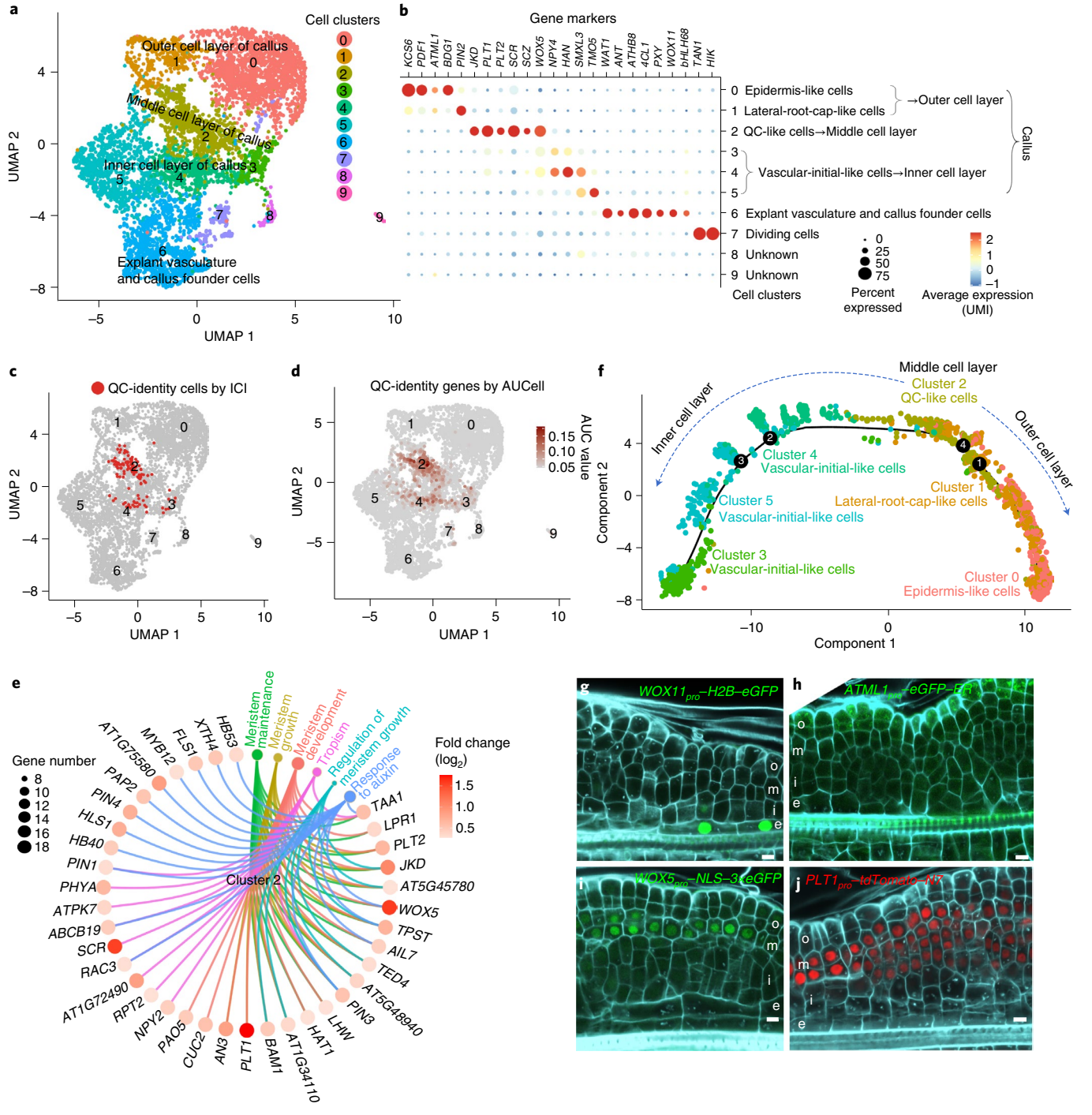

Fig. 1 | Single-cell RNA-seq analysis of callus. a, UMAP of cell clusters 0 to 9 in single-cell RNA-seq of callus from *Arabidopsis* hypocotyl explants at six days. Also see Supplementary Fig. 1. **b**, Dot plot of marker genes showing the cell identities of each cell cluster. Average expression indicates normalized and scaled unique molecular identifiers (UMI). **c**,**d**, UMAP of cells showing QC identity by ICI (**c**) and AUCell (**d**) analyses. We used an information-theory-based approach to analyse the ICI scores by calculating the relative contributions of 15 root tissue identities in each cell from the single-cell RNA-seq data[14], and we found that there were 122 cells harbouring the QC identity (**c**). For AUCell[15], there are 91 genes specifically expressed in *AGL42*-positive cells (that is, QC cells)[16], and we identified 84 out of the 91 genes in the single-cell RNA-seq data (**d**). Note that QC identity was identified primarily in cells from cluster 2 and also in a small portion of cells in clusters 3 and 4. **e**, GO analysis of enriched genes in cell cluster 2. The top six GO terms and selected genes are shown. Gene number indicates the number of cluster-2 marker genes in the GO term analysis. Fold change indicates the upregulated expression level of the gene in cluster 2 compared with that in other clusters. See Supplementary Table 1 for genes enriched in cell cluster 2 and Supplementary Table 2 for the full list of the GO analysis. **f**, Simulation of the successive differentiation trajectory of the three layers of callus (clusters 0 to 5) over pseudo-time. The numbers indicate branching points. The arrows indicate two directions of predicted differentiation routes. **g**–**j**, Expression patterns of *WOX11*$_{pro}$*–H2B–GFP* (**g**), *ATML1*$_{pro}$*–eGFP–ER* (**h**), *WOX5*$_{pro}$*–NLS–3×eGFP* (**i**) and *PLT1*$_{pro}$*–tdTomato–N7* (**j**) in callus on CIM at six to seven days. Note that *WOX11* expression in the vasculature of explants might indicate continuous production of callus on CIM. Calcofluor White was used to indicate cell walls. o, outer cell layer; m, middle cell layer; i, inner cell layer; e, explant vasculature. Two biological repeats were analysed and showed similar results. Scale bars, 10 μm in **g**–**j**.

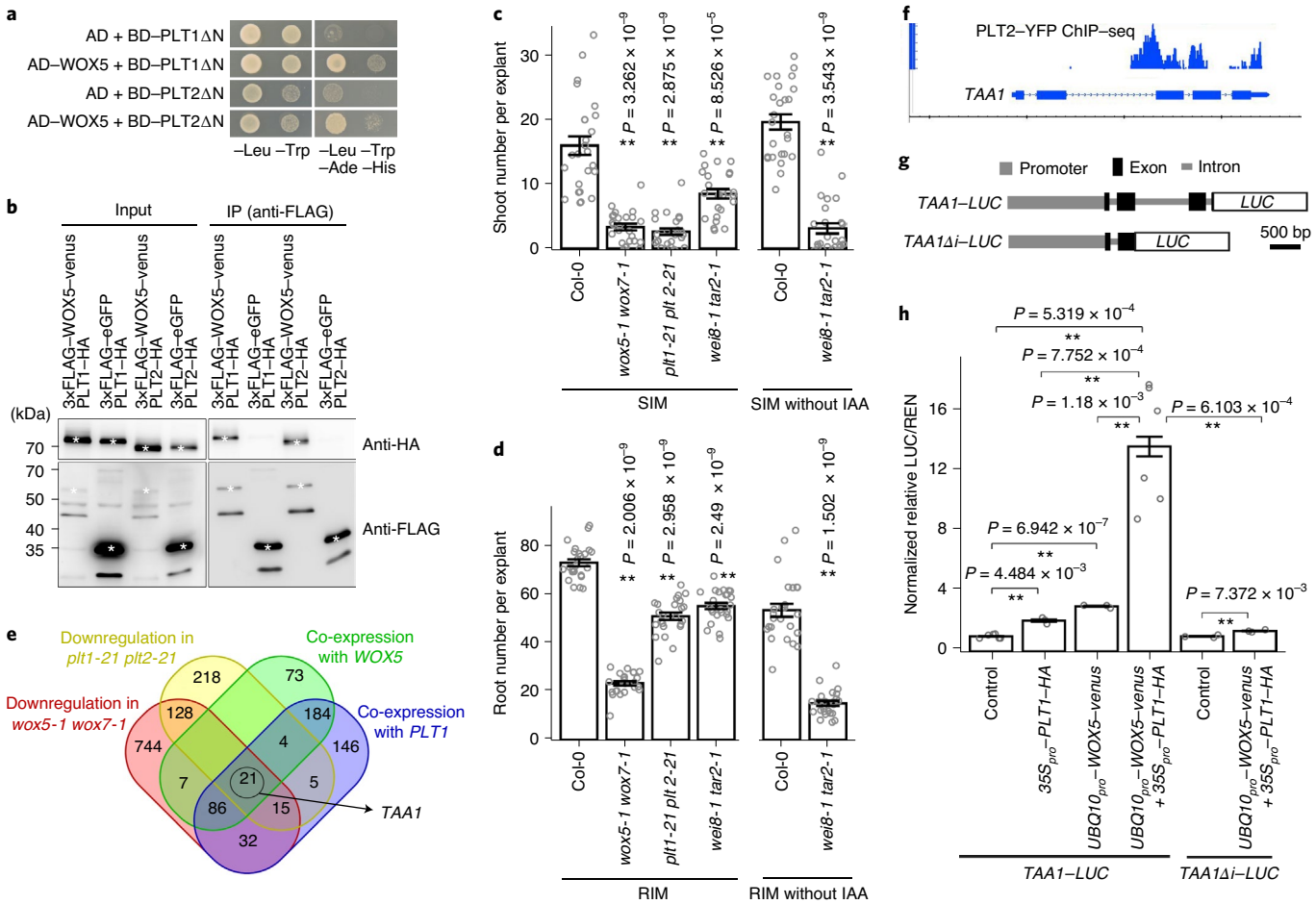

Fig. 2 | *WOX5/7* promote auxin production in callus. a, Yeast two-hybrid analysis of the interaction between WOX5 and PLT1/2. ΔN indicates the deletion of the N-terminal region[61]. Two biological repeats were analysed and showed similar results. AD, activation domain; BD, binding domain; Ade, adenine. **b**, Co-IP analysis of the interaction between WOX5 and PLT1/2 in *Arabidopsis* protoplasts transformed with $UBQ10_{pro}$–3×*FLAG*–*WOX5*–*Venus* with $35S_{pro}$–*PLT1*–*HA* or $35S_{pro}$–*PLT2*–*HA*. $UBQ10_{pro}$–3×*FLAG*–*eGFP* served as the control. The white asterisks indicate HA- or FLAG-fused proteins. Two biological repeats were analysed and showed similar results. **c**,**d**, Statistical analyses of shoot formation on SIM at 12 days (**c**) and root formation on RIM at 8 days (**d**) in Col-0, *wox5-1 wox7-1*, *plt1-21 plt2-21* and *wei8-1 tar2-1*. Calli were cultured on CIM for 5 days and then moved to SIM or RIM. IAA, indole acetic acid. The data are presented as mean values ± s.e.m. ($n = 24$ explants). The individual values are indicated by grey dots. $^{**}P < 0.01$ in a two-sided Mann–Whitney *U*-test compared with the Col-0 control. Also see Supplementary Fig. 1. **e**, Venn plot showing genes downregulated in *wox5-1 wox7-1* or *plt1-21 plt2-21* callus compared with Col-0 callus at six days, and genes co-expressed with *WOX5* or *PLT1* in single-cell RNA-seq data. See Supplementary Tables 3 and 4 for the list of RNA-seq data in *wox5-1 wox7-1* and *plt1-21 plt2-21* callus, respectively. **f**, Chromatin immunoprecipitation sequencing (ChIP–seq) results of PLT2–YFP on the *TAA1* locus shown by previously published data[36]. **g**, Diagram of *TAA1–LUC* and *TAA1Δi–LUC* constructs. *Δi* represents the deletion of the intron of *TAA1*. **h**, Relative ratio of firefly LUC to *Renilla* luciferase (REN) activity in *Arabidopsis* protoplasts co-transformed with *TAA1–LUC* or *TAA1Δi–LUC* with $35S_{pro}$–*PLT1–HA*, $UBQ10_{pro}$–*WOX5–Venus* or $35S_{pro}$–*PLT1–HA* + $UBQ10_{pro}$–*WOX5–Venus*. The data are presented as mean values ± s.e.m. from more than three biological replicates. Each biological replicate was analysed with two technical replicates. The individual values are indicated by dots. $^{**}P < 0.01$ in a two-sided Student's *t*-test with the control.

plt1-21 plt2-21 in RNA-seq data (Supplementary Tables 3 and 4) and co-expressed in the cells expressing *WOX5* and *PLT1* in single-cell RNA-seq (Fig. 2e and Supplementary Table 5), and the auxin biosynthesis gene *TRYPTOPHAN AMINOTRANSFERASE OF ARABIDOPSIS1* (*TAA1*) was on the list (Fig. 2e and Supplementary Fig. 4). Quantitative PCR with reverse transcription (RT–qPCR) confirmed that the *TAA1* expression level was reduced in callus from *wox5-1 wox7-1* or *plt1-21 plt2-21* compared with callus from Col-0 (Supplementary Fig. 4). Mutations in *TAA1* and its redundant homologue *TAR2* (the *wei8-1 tar2-1* double mutant) showed defective shooting and rooting from callus (Fig. 2c,d), and this defect was more severe when exogenous auxin was not added in SIM or RIM (Fig. 2c,d). PLT2 was shown to directly bind the intron of *TAA1* (ref. [36]) (Fig. 2f). Our data showed that PLT1 and WOX5 could act synergistically to activate *TAA1* expression through its intron (Fig. 2g,h). The upregulation of endogenous auxin biosynthesis by the WOX5–PLT1/2 complex is therefore required for organ regeneration.

We further analysed the role of *WOX5/7* in the regulation of cytokinin response in the middle cell layer of callus. First, RNA-seq analysis of callus at six days on CIM derived from hypocotyl explants of wild-type Col-0 and the *wox5-1 wox7-1* double mutant (Supplementary Table 3) showed that in addition to their roles in maintenance of the undifferentiated stem cell status, *WOX5/7* could repress the expression of A-type *ARR*s (Fig. 3a and Supplementary Fig. 5). Observations of the $ARR5_{pro}$–*eGFP* reporter line (Fig. 3b) confirmed that the A-type *ARR5* transcript level was higher in *wox5-1 wox7-1* callus than in Col-0 callus on CIM and SIM. Second,

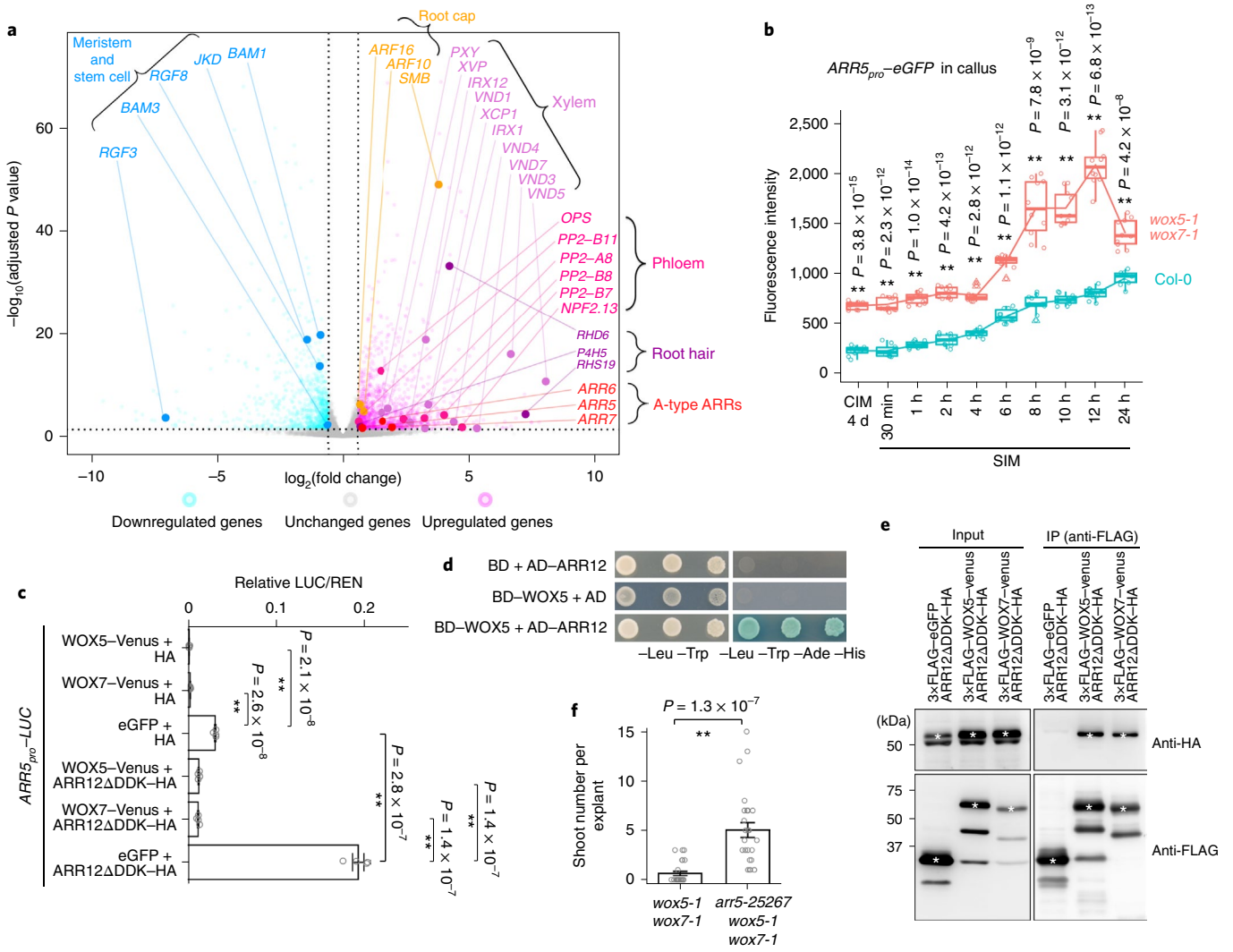

Fig. 3 | *WOX5/7* promote cytokinin signalling in callus. a, RNA-seq analysis of gene transcript profiles in six-day-old callus derived from Col-0 and *wox5-1 wox7-1* hypocotyl explants on CIM. Genes with lower transcript levels in *wox5-1 wox7-1* than in Col-0 contained meristem and stem-cell-related genes. Genes with higher transcript levels in *wox5-1 wox7-1* than in Col-0 contained xylem-related genes, phloem-related genes, root-hair-related genes, root-cap-related genes, and A-type *ARR5*, *6* and *7* in the cytokinin signalling pathway (see Supplementary Table 3 for a detailed description). **b**, Statistical analysis of $ARR5_{pro}$*–eGFP* fluorescence intensity in callus derived from Col-0 and *wox5-1 wox7-1* hypocotyl explants on CIM and SIM. Fluorescence intensity was quantified by NIS-Elements AR v.5.10 (Nikon). The box bounds indicate the interquartile range (25th to 75th percentiles), the centre line indicates the median, the whiskers indicate 1.5× the interquartile range from the lower and upper bounds, and the outliers are indicated by triangles. The individual values are indicated by dots. $n = 10$ calli in each box. **c**, Relative ratio of firefly LUC to REN activity in *Arabidopsis* protoplasts co-transformed with $ARR5_{pro}$*–LUC* with $UBQ10_{pro}$*–WOX5–Venus* + $35S_{pro}$*–HA*, $UBQ10_{pro}$*–WOX7–Venus* + $35S_{pro}$*–HA*, $UBQ10_{pro}$*–eGFP* + $35S_{pro}$*–HA*, $UBQ10_{pro}$*–WOX5–Venus* + $35S_{pro}$*–ARR12ΔDDK–HA*, $UBQ10_{pro}$*–WOX7–Venus* + $35S_{pro}$*–ARR12ΔDDK–HA* or $UBQ10_{pro}$*–eGFP* + $35S_{pro}$*–ARR12ΔDDK–HA*. ΔDDK represents the deletion of the DDK domain, resulting in the activation of ARR12 function without the control of cytokinin[59]. The data are presented as mean values ± s.e.m. from four biological replicates. Each biological replicate was analysed with two technical replicates. The individual values are indicated by dots. **d**, Yeast two-hybrid analysis of the interaction between WOX5 and ARR12. Two biological repeats were analysed and showed similar results. **e**, Co-IP analysis of the interaction between WOX5 and ARR12 in *Arabidopsis* protoplasts transformed with $UBQ10_{pro}$*–3×FLAG–WOX5–Venus* or $UBQ10_{pro}$*–3×FLAG–WOX7–Venus* with $35S_{pro}$*–ARR12ΔDDK–HA*. $UBQ10_{pro}$*–3×FLAG–eGFP* served as the control. The white asterisks indicate HA- or FLAG-fused proteins. Two biological repeats were analysed and showed similar results. **f**, Statistical analysis of shoot regeneration on SIM at 12 days from calli of *wox5-1 wox7-1* and *arr5-25267 wox5-1 wox7-1*. Calli were cultured on CIM for 5 days and then moved to SIM. The data are presented as mean values ± s.e.m. from 25 explants. The individual values are indicated by dots. $^{**}P < 0.01$ in a two-sided Student's *t*-test (**b**,**c**) or Mann–Whitney *U*-test (**f**).

WOX5/7 could inhibit A-type *ARR5* expression in *Arabidopsis* protoplasts (Fig. 3c). Third, it is known that B-type ARRs can directly activate the expression of A-type *ARR*s upon cytokinin induction, and then A-type ARRs inhibit cytokinin signalling mediated by B-type ARRs, therefore forming a negative feedback loop[37,38]. Among B-type *ARR*s, *ARR12* is known to be the major player in callus formation and shoot regeneration in tissue culture[39–42] and was ubiquitously expressed in all three cell layers in callus on CIM (Supplementary Fig. 6). We therefore explored the roles of B-type *ARR12* and *WOX5/7* in the regulation of A-type *ARR5* in *Arabidopsis* protoplasts. The results showed that *ARR12* could upregulate *ARR5*, but this upregulation was inhibited by the co-expression of

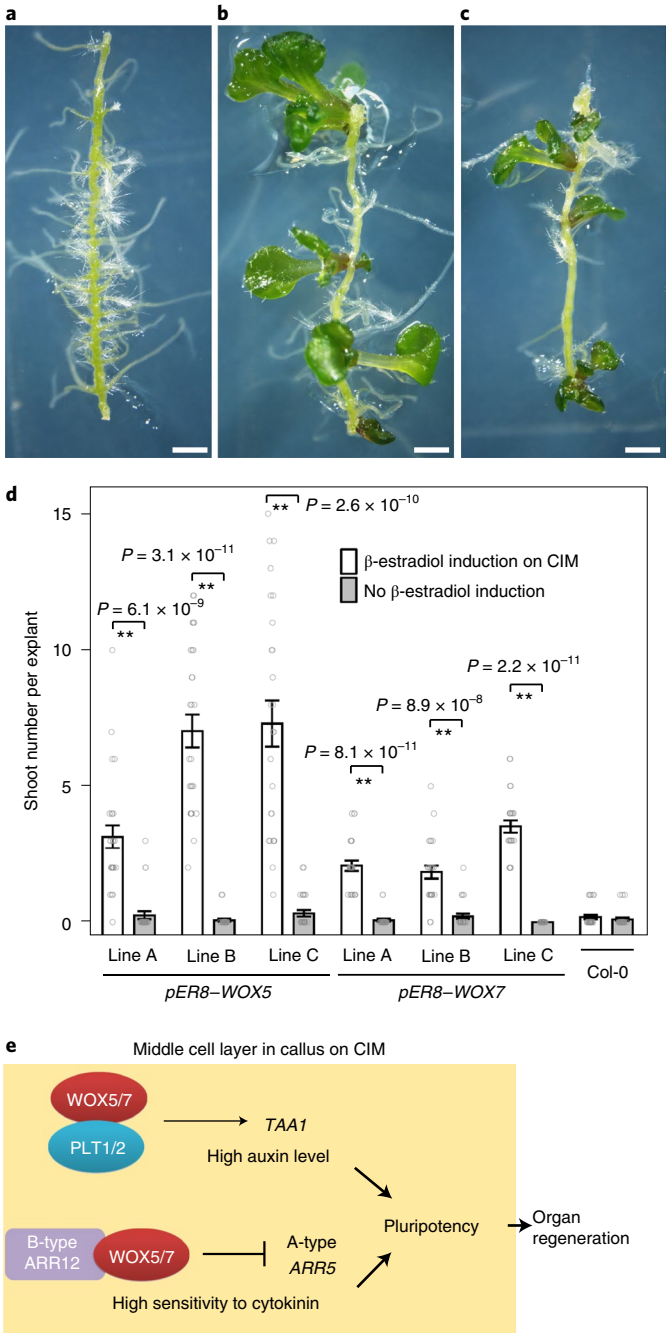

Fig. 4 | Overexpression of *WOX5* or *WOX7* promotes shoot regeneration. **a**–**d**, Phenotype (Col-0, **a**; *pER8–WOX5*, **b**; *pER8–WOX7*, **c**) and statistical (**d**) analyses of shoot regeneration on low-cytokinin medium (Murashige and Skoog (MS) basal medium with vitamins, 2% w/v sucrose, 0.1 μM 6-(γ,γ-dimethylallylamino) purine, 0.9 μM IAA). Hypocotyl explants of *pER8–WOX5* or *pER8–WOX7* were cultured on CIM for 6 days without or with 10 μM β-estradiol induction, and then calli were moved to low-cytokinin medium without β-estradiol and further cultured for 14 days. Col-0 served as a control. Scale bars, 1 mm in **a**–**c**. In **d**, the data are presented as mean values ± s.e.m. from 25 explants, and the individual values are indicated by dots. $^{**}P < 0.01$ in a two-sided Mann–Whitney *U*-test compared with the Col-0 control. **e**, Model of the middle cell layer of callus in organ regeneration.

ARR12 with *WOX5* or *WOX7* (Fig. 3c). Fourth, yeast two-hybrid and Co-IP data showed that WOX5/7 could directly interact with B-type ARR12 (Fig. 3d,e). WOX5 could also interact with B-type ARR2 in the yeast two-hybrid assay (Supplementary Fig. 7). Fifth, a mutation in *ARR5* could partially rescue the defective shoot formation in *wox5-1 wox7-1* callus (Fig. 3f), suggesting that the shoot regeneration defect in *wox5-1 wox7-1* might be at least partially due to the over-accumulation of *ARR5* in callus. However, A-type *ARR5* mutation could not rescue the rooting defect in *wox5-1 wox7-1* on RIM (Supplementary Fig. 8). Taken together, these results indicated that WOX5/7 might promote cytokinin response by breaking the negative feedback loop of cytokinin signalling.

To test whether WOX5/7 might serve as a regeneration-promoting factor in tissue culture, we analysed transgenic plants expressing *WOX5* or *WOX7* under the control of a β-estradiol-inducible promoter (*pER8–WOX5* and *pER8–WOX7* transgenic plants). Overexpression of *WOX5* or *WOX7* was induced by β-estradiol in callus on CIM, and then the callus was moved to a β-estradiol-free medium with a lower cytokinin level than that in SIM. The results showed that callus of *pER8–WOX5* or *pER8–WOX7* induced by β-estradiol on CIM regenerated shoots on medium with a low cytokinin level, while callus of *pER8–WOX5* or *pER8–WOX7* without β-estradiol induction or callus of the wild-type control could barely regenerate shoots (Fig. 4a–d). However, overexpression of *WOX5* or *WOX7* could not promote root regeneration on RIM (Supplementary Fig. 9). These results showed that *WOX5* or *WOX7* overexpression can enhance the cytokinin sensitivity of callus cells to promote shoot regeneration.

Here, we propose a model of pluripotency acquisition during callus formation on CIM (Fig. 4e). At the cellular level, callus comprises a group of heterogeneous cells and resembles root primordium or RAM. The cells expressing the QC-identity gene network within the middle cell layer could be primarily responsible for organ regeneration. However, the middle cell layer is not equal to the QC. For example, the middle cell layer in callus undergoes active cell division, while the QC cells in RAM are not highly active in division. In addition, the transcriptome of the middle cell layer is similar to that of the QC, but there are still some differences between them (Fig. 1d). At the molecular level, WOX5/7 might promote regeneration via at least via two pathways: (1) WOX5/7 interact with PLT1/2 to promote *TAA1* for endogenous auxin production in callus to maintain a high auxin level, and (2) WOX5/7 interact with ARR12 and repress *ARR5*, leading to high sensitivity to cytokinin by removing the negative feedback mechanism in cytokinin signalling. The high auxin level might function in maintenance of the pluripotency in the middle cell layer of callus on CIM and promote RAM regeneration when callus is moved to RIM. It is possible that QC-like identity establishment and local auxin production might be common underlying principles of pluripotency acquisition both in callus from tissue culture and in tissue repair of wounded organs[43–46]. The high sensitivity to cytokinin could be important for the activation of the shoot-progenitor-controlling genes by cytokinin when callus is moved to SIM. When *WUS* is expressed in shoot progenitor cells and *WOX5/7* expression decreases on SIM, *WOX5/7* could pass the role of A-type *ARR* repression to *WUS* to establish the shoot apical meristem[47]. Besides the role of WOX5/7 in the regulation of *TAA1* and *ARR*s on CIM, there could be other factors that regulate auxin production and *ARR*s on RIM and SIM[30,39,45,48,49]. Overall, our study indicates that the middle cell layer of callus from hypocotyl explants on CIM has the QC-like transcriptional identity and is pluripotent for organ regeneration. There are many types of callus in plants, and they have different cellular features[50]. It will be interesting to test how different types of callus undergo regeneration in the future.

Methods

Plant materials and culture conditions. *Arabidopsis* Col-0 was the wild type in this study. The lines *wox5-1 wox7-1* (ref. [51]), *plt1-21* (SALK_116254)[52], *plt2-21* (GK-297D04-015553), *arr5-25267* (CS25267)[38,53], *wei8-1 tar2-1* (ref. [54]), $ATML1_{pro}$–*eGFP–ER*[30], $ARR5_{pro}$–*eGFP*[30], $TCSn_{pro}$–*mGFP5–ER*[55], WUS_{pro}–*3×Venus–N7* (ref. [42]) and $TAA1_{pro}$–*TAA1–GFP*[56] have been described previously or in this study.

To generate *WOX11*$_{pro}$*–H2B–eGFP*, *WOX5*$_{pro}$*–NLS–3×eGFP*, *PLT1*$_{pro}$*–tdTomato–N7* and *ARR12*$_{pro}$*–gARR12–Venus*, the 5-kb, 4.8-kb and 5.7-kb promoters of *WOX11*, *WOX5* and *PLT1* and the 7.5-kb genomic region including the promoter and the gene body of *ARR12* were cloned into *pBI101–H2B–eGFP*, *pBI101–NLS–3×eGFP*, *pBI101–tdTomato–N7* and *pBI101–Venus* (all modified from pBI101), respectively. The constructs were introduced into Col-0 by *Agrobacterium tumefaciens*-mediated transformation.

For tissue culture, *Arabidopsis* seeds were sterilized with 75% ethanol and then germinated vertically and grown on 1/2 MS basal medium without sucrose at 22 °C under dark conditions for nine days. The hypocotyl explants (~1 cm in length) were cut and cultured on CIM (MS basal medium with vitamins, 2% w/v sucrose, 11 μM 2,4-dichlorophenoxyacetic acid, 0.2 μM kinetin) under 24-h light conditions at 22 °C for five to seven days. The calli were then transferred to SIM (MS basal medium with vitamins, 2% w/v sucrose, 1 μM 6-(γ,γ-dimethylallylamino) purine, 0.9 μM IAA) or RIM (MS basal medium with vitamins, 2% w/v sucrose, 0.9 μM IAA) under 24-h light conditions at 22 °C.

RT–qPCR and dual-luciferase, Co-IP and yeast two-hybrid assays. RT–qPCR was carried out as previously described[57]. The RT–qPCR results are presented as relative transcript levels, normalized against that of *AT1G13320* (ref. [58]).

For the dual-luciferase and Co-IP assays, the full-length complementary DNA of *PLT1* or *PLT2* fused with the HA tag was cloned into pMD19T under the control of the 35S promoter to generate *35S*$_{pro}$*–PLT1–HA* and *35S*$_{pro}$*–PLT2–HA*. The region 1.5 kb upstream and 1.8 kb downstream of ATG from the *TAA1* locus was cloned into the pAB287 vector, which contains a firefly luciferase gene, to generate *TAA1–LUC*. For *TAA1Δi–LUC*, the region 1.5 kb upstream and 508 bp downstream of ATG from the *TAA1* locus was cloned into pAB287. The cDNA encoding amino acids 131–596 of ARR12 without the DDK domain[59] fused with an HA tag was cloned into pMD19T under the control of the 35S promoter to generate *35S*$_{pro}$*–ARR12ΔDDK–HA*. The cDNAs encoding *WOX5–Venus*, *3×FLAG–WOX5–Venus*, *WOX7–Venus*, *3×FLAG–WOX7–Venus*, *eGFP* and *3×FLAG–eGFP* were cloned into the pMD19T vector under the control of the *UBQ10* promoter to generate *UBQ10*$_{pro}$*–WOX5–Venus*, *UBQ10*$_{pro}$*–3×FLAG–WOX5–Venus*, *UBQ10*$_{pro}$*–WOX7–Venus*, *UBQ10*$_{pro}$*–3×FLAG–WOX7–Venus*, *UBQ10*$_{pro}$*–eGFP* and *UBQ10*$_{pro}$*–3×FLAG–eGFP*, respectively. The 1.7-kb promoter of *ARR5* was cloned into the pAB287 vector to generate *ARR5*$_{pro}$*–LUC*. The dual-luciferase assay was carried out in *Arabidopsis* protoplasts[60] using the Dual-Luciferase Reporter Assay System (Promega). *UBQ10*$_{pro}$*–Rluc* was used as the normalization control. For the Co-IP assays, plasmids (50 μg each) were transformed into 5×10^5 *Arabidopsis* protoplasts[60]. The protoplasts were collected, and total proteins were extracted using lysis buffer (50 mM Tris, pH 7.4; 150 mM NaCl; 1 mM EDTA; 5% v/v glycerol; 1% v/v Triton X-100) after 12 h. Total extracts were cleared by centrifuging twice at 4 °C at 18,506*g*. Immunoprecipitation was performed using anti-FLAG affinity gel (A2220; Sigma) followed by washing five times with lysis buffer. Proteins were eluted by SDS–PAGE loading buffer at 95 °C. Western blot analyses were performed using the anti-HA antibody (H6533; Sigma) with 1:5,000 dilution and anti-FLAG antibody (A8592; Sigma) with 1:5,000 dilution.

For the yeast two-hybrid assays, cDNAs encoding *WOX5*, *ARR12*, *ARR2*, *PLT1ΔN* (180–575 amino acids)[61] and *PLT2ΔN* (189–569 amino acids)[61] were cloned into pGBKT7 and pGADT7. The yeast two-hybrid assays were performed as described previously[62].

The primers used for RT–qPCR and molecular cloning are listed in Supplementary Table 6.

ClearSee, microscopy and CRE/LOX analysis. The ClearSee assays were performed as previously described[31]. In brief, plant materials were immersed in fixation buffer (4% w/v paraformaldehyde in 1× PBS) under vacuum at 37 mbar for 30 min. After fixation for 12 h, the explants were washed once with 1× PBS and then cleared in ClearSee reagent[31] for one week. After staining in Calcofluor White (1 mg ml^{-1} in ClearSee reagent) for 12 h, the plant materials were immersed in ClearSee reagent and observed under a Nikon C2 inverted confocal microscope using a 488-nm laser for GFP and Venus, a 561-nm laser for tdTomato, and a 405-nm laser for Calcofluor White. Analysis of CRE/LOX driven by the *WOX5* promoter was carried out as previously described[32].

RNA-seq. Total RNA was extracted from six-day-old calli on CIM derived from Col-0, *wox5-1 wox7-1* and *plt1-21 plt2-21* hypocotyl explants, and RNA-seq was performed using the Illumina HiSeq 3000 platform (Genergy Biotechnology). Mapping of reads to the *A. thaliana* genome (TAIR10) and transcript counting were conducted using STAR v.2.7.2b[63]. Differentially expressed genes (DEGs) were determined by DESeq2 (ref. [64]). Two biological replicates were used in the data analyses.

Single-cell RNA-seq. The hypocotyl explants were cultured on CIM for six days. The epidermis and cortex of the explants were removed, and the callus together with the vasculature of the explants were collected for single-cell RNA-seq. About 150 Col-0 calli were incubated in digestion buffer (0.8 M sorbitol, 10 mM MES, 1.5% Cellulase RS, 1% Macerozyme R10, 1 mM $CaCl_2$, 0.1% w/v BSA, 0.03% v/v β-mercaptoethanol, pH 5.7) for 1 h at room temperature and then dissected under a microscope to release protoplasts. The protoplast solution was strained through a 40-μm filter. The filtered solution was centrifuged at 500*g* for 3 min and then washed once with resuspension buffer (12% w/v sorbitol and 0.05% w/v BSA) at 4 °C. The protoplast pellet was resuspended in 125 μl of resuspension buffer and stored on ice. About 99% cell viability was confirmed by AO/PI staining.

These cells were captured by the BD Rhapsody system (https://www.bdbiosciences.com/), and the libraries were sequenced by an Illumina NovaSeq sequencer (NovelBio Bio-Pharm Technology Co.). The adaptor sequence and the low-quality reads were filtered by fastp with the default parameters[65]. UMI-tools were applied for single-cell transcriptome analysis to identify the cell barcode whitelist[66]. The UMI-based clean data were mapped to the *A. thaliana* genome (TAIR10) utilizing STAR mapping with customized parameters from the UMI-tools standard pipeline to obtain the UMI counts of each sample[63].

Seurat v.3.0 (https://satijalab.org/seurat/) was used for filtering the data, reducing dimensions, clustering cells and identifying DEGs[67]. The UMI expression matrix with genes expressed in at least 5 cells and cells expressing at least 200 genes was loaded into Seurat. Further cleaning steps were performed using nCount within twofold standard deviation, nFeature within twofold standard deviation and mitochondria percentage below 5%. A total of 5,913 cells with averages of 11,379 UMIs and 3,954 genes after filtering were used for downstream analysis. The SCTransform function with the default parameters was used for data normalization, scaling and transformation. Because callus was highly active in cell division, we mitigated the cell cycle effects on clustering by performing cell cycle regression using *Arabidopsis* G2/M and S specific genes[68,69] (Supplementary Table 7). After running the CellCycleScoring function, SCTransform was performed again to regress out cell cycle effects by defining vars.to.regress augments with S.Score and G2M.Score. Although cells in the S phase were regressed out, we could still observe some cells with high G2M scores enriched in cluster 7. The dimensions of the expression matrix were then reduced by the RunPCA function, and the top 30 dimensions were used for FindNeighbors and UMAP analysis[2]. The cell clusters were identified by the FindClusters function with a resolution of 0.8. Calculations for the DEGs were conducted using the FindAllMarkers function with the default parameters. On the basis of the DEGs among different clusters and CLSM results of marker genes, we combined all clusters into ten clusters. The marker genes of each cluster were identified using FindAllMarkers with the Wilcox rank sum test algorithm under following criteria: avg_log$_2$FC > 0.25, p_val_adj < 0.05, pct1 > 0.1 and pct2 < 0.5 (ref. [70]).

The marker genes of cluster 2 were used for GO enrichment analysis with all genes filtered by Seurat serving as background. The GO analysis was performed using the enrichGO function in clusterProfiler[71]. The top six significant terms were visualized via the cnetplot function[71] in Fig. 1e.

For the co-expression analysis, we extracted cells with candidate genes UMI > 0. The Seurat function of FindMarkers with the Wilcox rank sum test algorithm was used to identify the enriched genes.

ICI[14] and AUCell[15,16] were used to identify cells with QC identity. For ICI, we used the spec value from QC markers with MIN_USEFUL_SPEC = 0.15, and significance values were calculated with 1,000 times bootstrapping. The cells with p_adj < 0.05 were highlighted in the UMAP plot in Fig. 1c. For AUCell, we used the *AGL42* marker gene list[16] to calculate the area under the recovery curve (AUC) value. The AUC threshold was calculated by the getThresholdSelected function with the default parameters. The AUC values higher than the threshold (0.04634622) were mapped to the UMAP plot in Fig. 1d.

To construct the pseudo-time development trajectory, raw counts of cells from clusters 0 to 5 were extracted and used for the Monocle2 v.2.18.0 algorithm in R[72]. The genes with a mean expression value ≥0.011 and a dispersion empirical value larger than the dispersion fit value were used for ordering cells. The cells were ordered along the trajectory and visualized in a reduced dimensional space by the DDRTree algorithm[72]. The root_state augment was modified to cluster 2.

Reporting Summary. Further information on research design is available in the Nature Research Reporting Summary linked to this article.

Data availability

The sequence data can be accessed at the Arabidopsis Genome Initiative (https://www.arabidopsis.org/) under the following accession numbers: *WOX11* (AT3G03660), *WOX5* (AT3G11260), *WOX7* (AT5G05770), *PLT1* (AT3G20840), *PLT2* (AT1G51190), *SCR* (AT3G54220), *ARR5* (AT3G48100), *ARR7* (AT1G19050), *ARR12* (AT2G25180), *ARR2* (AT4G16110), *WUS* (AT2G17950), *JKD* (AT5G03150), *TAA1* (AT1G70560), *TAR2* (AT4G24670), *KCS6* (AT1G68530), *PDF1* (AT2G42840), *ATML1* (AT4G21750), *BDG1* (AT1G64670), *PIN2* (AT5G57090), *SCZ* (AT1G46264), *NPY4* (AT2G23050), *HAN* (AT3G50870), *SMXL3* (AT3G52490), *TMO5* (AT3G25710), *WAT1* (AT1G75500), *ANT* (AT4G37750), *ATHB8* (AT4G32880), *4CL1* (AT1G51680), *PXY* (AT5G61480), *bHLH068* (AT4G29100), *TAN1* (AT3G05330) and *HIK* (AT1G18370). The RNA-seq and single-cell RNA-seq data have been deposited in the Gene Expression Omnibus (http://www.ncbi.nlm.nih.gov/geo) under the accession numbers GSE156990, GSE178354 and GSE156991. The RNA-seq and single-cell RNA-seq data can be accessed using the online tool (http://xulinlab.cemps.ac.cn/), and gene IDs can be used to search for gene expression patterns. The data that support the findings of this study are available from the corresponding author upon request. Source data are provided with this paper.

Received: 2 September 2020; Accepted: 5 October 2021;
Published online: 15 November 2021

References

1. Ikeuchi, M. et al. Molecular mechanisms of plant regeneration. *Annu. Rev. Plant Biol.* **70**, 377–406 (2019).
2. Becht, E. et al. Dimensionality reduction for visualizing single-cell data using UMAP. *Nat. Biotechnol.* **37**, 38–44 (2019).
3. Sugimoto, K., Jiao, Y. & Meyerowitz, E. M. *Arabidopsis* regeneration from multiple tissues occurs via a root development pathway. *Dev. Cell* **18**, 463–471 (2010).
4. Trinh, D.-C. et al. PUCHI regulates very long chain fatty acid biosynthesis during lateral root and callus formation. *Proc. Natl Acad. Sci. USA* **116**, 14325–14330 (2019).
5. Abe, M., Takahashi, T. & Komeda, Y. Identification of a *cis*-regulatory element for L1 layer-specific gene expression, which is targeted by an L1-specific homeodomain protein. *Plant J.* **26**, 487–494 (2001).
6. Kurdyukov, S. et al. The epidermis-specific extracellular BODYGUARD controls cuticle development and morphogenesis in *Arabidopsis*. *Plant Cell* **18**, 321–339 (2006).
7. Sessions, A., Weigel, D. & Yanofsky, M. F. The *Arabidopsis thaliana* MERISTEM LAYER 1 promoter specifies epidermal expression in meristems and young primordia. *Plant J.* **20**, 259–263 (1999).
8. Benková, E. et al. Local, efflux-dependent auxin gradients as a common module for plant organ formation. *Cell* **115**, 591–602 (2003).
9. Di Laurenzio, L. et al. The SCARECROW gene regulates an asymmetric cell division that is essential for generating the radial organization of the *Arabidopsis* root. *Cell* **86**, 423–433 (1996).
10. ten Hove, C. A. et al. SCHIZORIZA encodes a nuclear factor regulating asymmetry of stem cell divisions in the *Arabidopsis* root. *Curr. Biol.* **20**, 452–457 (2010).
11. Welch, D. et al. Arabidopsis JACKDAW and MAGPIE zinc finger proteins delimit asymmetric cell division and stabilize tissue boundaries by restricting SHORT-ROOT action. *Genes Dev.* **21**, 2196–2204 (2007).
12. Aida, M. et al. The PLETHORA genes mediate patterning of the *Arabidopsis* root stem cell niche. *Cell* **119**, 109–120 (2004).
13. Sarkar, A. K. et al. Conserved factors regulate signalling in *Arabidopsis thaliana* shoot and root stem cell organizers. *Nature* **446**, 811–814 (2007).
14. Efroni, I., Ip, P.-L., Nawy, T., Mello, A. & Birnbaum, K. D. Quantification of cell identity from single-cell gene expression profiles. *Genome Biol.* **16**, 9 (2015).
15. Aibar, S. et al. SCENIC: single-cell regulatory network inference and clustering. *Nat. Methods* **14**, 1083–1086 (2017).
16. Brady, S. M. et al. A high-resolution root spatiotemporal map reveals dominant expression patterns. *Science* **318**, 801–806 (2007).
17. De Rybel, B. et al. A bHLH complex controls embryonic vascular tissue establishment and indeterminate growth in *Arabidopsis*. *Dev. Cell* **24**, 426–437 (2013).
18. Cheng, Y., Qin, G., Dai, X. & Zhao, Y. NPY genes and AGC kinases define two key steps in auxin-mediated organogenesis in *Arabidopsis*. *Proc. Natl Acad. Sci. USA* **105**, 21017–21022 (2008).
19. Nawy, T. et al. The GATA factor HANABA TARANU is required to position the proembryo boundary in the early *Arabidopsis* embryo. *Dev. Cell* **19**, 103–113 (2010).
20. Wallner, E.-S. et al. Strigolactone- and karrikin-independent SMXL proteins are central regulators of phloem formation. *Curr. Biol.* **27**, 1241–1247 (2017).
21. Smetana, O. et al. High levels of auxin signalling define the stem-cell organizer of the vascular cambium. *Nature* **565**, 485–489 (2019).
22. Baima, S. et al. The expression of the Athb-8 homeobox gene is restricted to provascular cells in *Arabidopsis thaliana*. *Development* **121**, 4171–4182 (1995).
23. Etchells, J. P. & Turner, S. R. The PXY–CLE41 receptor ligand pair defines a multifunctional pathway that controls the rate and orientation of vascular cell division. *Development* **137**, 767–774 (2010).
24. Lee, D., Ellard, M., Wanner, L. A., Davis, K. R. & Douglas, C. J. The *Arabidopsis thaliana* 4-coumarate:CoA ligase (4CL) gene: stress and developmentally regulated expression and nucleotide sequence of its cDNA. *Plant Mol. Biol.* **28**, 871–884 (1995).
25. Ranocha, P. et al. WALLS ARE THIN 1 (WAT1), an *Arabidopsis* homolog of *Medicago truncatula* NODULIN21, is a tonoplast-localized protein required for secondary wall formation in fibers. *Plant J.* **63**, 469–483 (2010).
26. Zhang, Y. et al. Two types of bHLH transcription factor determine the competence of the pericycle for lateral root initiation. *Nat. Plants* **7**, 633–643 (2021).
27. Liu, J. et al. WOX11 and 12 are involved in the first-step cell fate transition during de novo root organogenesis in *Arabidopsis*. *Plant Cell* **26**, 1081–1093 (2014).
28. Tanaka, H. et al. The AtNACK1/HINKEL and STUD/TETRASPORE/AtNACK2 genes, which encode functionally redundant kinesins, are essential for cytokinesis in *Arabidopsis*. *Genes Cells* **9**, 1199–1211 (2004).
29. Walker, K. L., Müller, S., Moss, D., Ehrhardt, D. W. & Smith, L. G. *Arabidopsis* TANGLED identifies the division plane throughout mitosis and cytokinesis. *Curr. Biol.* **17**, 1827–1836 (2007).
30. Gordon, S. P. et al. Pattern formation during de novo assembly of the *Arabidopsis* shoot meristem. *Development* **134**, 3539–3548 (2007).
31. Kurihara, D., Mizuta, Y., Sato, Y. & Higashiyama, T. ClearSee: a rapid optical clearing reagent for whole-plant fluorescence imaging. *Development* **142**, 4168–4179 (2015).
32. Zhai, N. & Xu, L. CRE/LOX-based analysis of cell lineage during root formation and regeneration in *Arabidopsis*. *aBIOTECH* **1**, 153–156 (2020).
33. Burkart, R. C. et al. PLETHORA and WOX5 interaction and subnuclear localisation regulates *Arabidopsis* root stem cell maintenance. Preprint at *bioRxiv* https://doi.org/10.1101/818187 (2019).
34. Kareem, A. et al. PLETHORA genes control regeneration by a two-step mechanism. *Curr. Biol.* **25**, 1017–1030 (2015).
35. Kim, J.-Y. et al. Epigenetic reprogramming by histone acetyltransferase HAG1/AtGCN5 is required for pluripotency acquisition in *Arabidopsis*. *EMBO J.* **37**, e98726 (2018).
36. Santuari, L. et al. The PLETHORA gene regulatory network guides growth and cell differentiation in *Arabidopsis* roots. *Plant Cell* **28**, 2937–2951 (2016).
37. Kieber, J. J. & Schaller, G. E. Cytokinins. *Arabidopsis Book* **12**, e0168 (2014).
38. To, J. P. C. et al. Type-A *Arabidopsis* response regulators are partially redundant negative regulators of cytokinin signaling. *Plant Cell* **16**, 658–671 (2004).
39. Liu, Z. et al. The type-B cytokinin response regulator ARR1 inhibits shoot regeneration in an ARR12-dependent manner in *Arabidopsis*. *Plant Cell* **32**, 2271–2291 (2020).
40. Dai, X. et al. ARR12 promotes de novo shoot regeneration in *Arabidopsis thaliana* via activation of WUSCHEL expression. *J. Integr. Plant Biol.* **59**, 747–758 (2017).
41. Meng, W. J. et al. Type-B ARABIDOPSIS RESPONSE REGULATORs specify the shoot stem cell niche by dual regulation of WUSCHEL. *Plant Cell* **29**, 1357–1372 (2017).
42. Zhang, T.-Q. et al. A two-step model for de novo activation of WUSCHEL during plant shoot regeneration. *Plant Cell* **29**, 1073–1087 (2017).
43. Matosevich, R. et al. Local auxin biosynthesis is required for root regeneration after wounding. *Nat. Plants* **6**, 1020–1030 (2020).
44. Matosevich, R. & Efroni, I. The quiescent center and root regeneration. *J. Exp. Bot.* https://doi.org/10.1093/jxb/erab319 (2021).
45. Cheng, Z. J. et al. Pattern of auxin and cytokinin responses for shoot meristem induction results from the regulation of cytokinin biosynthesis by AUXIN RESPONSE FACTOR3. *Plant Physiol.* **161**, 240–251 (2013).
46. Radhakrishnan, D. et al. A coherent feed forward loop drives vascular regeneration in damaged aerial organs growing in normal developmental-context. *Development* **147**, dev185710 (2020).
47. Leibfried, A. et al. WUSCHEL controls meristem function by direct regulation of cytokinin-inducible response regulators. *Nature* **438**, 1172–1175 (2005).
48. Ishihara, H. et al. Primed histone demethylation regulates shoot regenerative competency. *Nat. Commun.* **10**, 1786 (2019).
49. Yang, W., Choi, M.-H., Noh, B. & Noh, Y.-S. De novo shoot regeneration controlled by HEN1 and TCP3/4 in *Arabidopsis*. *Plant Cell Physiol.* **61**, 1600–1613 (2020).
50. Ikeuchi, M., Sugimoto, K. & Iwase, A. Plant callus: mechanisms of induction and repression. *Plant Cell* **25**, 3159–3173 (2013).
51. Hu, X. & Xu, L. Transcription factors WOX11/12 directly activate WOX5/7 to promote root primordia initiation and organogenesis. *Plant Physiol.* **172**, 2363–2373 (2016).
52. Kanei, M., Horiguchi, G. & Tsukaya, H. Stable establishment of cotyledon identity during embryogenesis in *Arabidopsis* by ANGUSTIFOLIA3 and HANABA TARANU. *Development* **139**, 2436–2446 (2012).
53. Huang, X. et al. The antagonistic action of abscisic acid and cytokinin signaling mediates drought stress response in *Arabidopsis*. *Mol. Plant* **11**, 970–982 (2018).
54. Stepanova, A. N. et al. TAA1-mediated auxin biosynthesis is essential for hormone crosstalk and plant development. *Cell* **133**, 177–191 (2008).
55. Zürcher, E. et al. A robust and sensitive synthetic sensor to monitor the transcriptional output of the cytokinin signaling network in planta. *Plant Physiol.* **161**, 1066–1075 (2013).
56. Wang, Q. et al. A phosphorylation-based switch controls TAA1-mediated auxin biosynthesis in plants. *Nat. Commun.* **11**, 679 (2020).
57. He, C., Chen, X., Huang, H. & Xu, L. Reprogramming of H3K27me3 is critical for acquisition of pluripotency from cultured *Arabidopsis* tissues. *PLoS Genet.* **8**, e1002911 (2012).
58. Czechowski, T., Stitt, M., Altmann, T., Udvardi, M. K. & Scheible, W.-R. Genome-wide identification and testing of superior reference genes for transcript normalization in *Arabidopsis*. *Plant Physiol.* **139**, 5–17 (2005).
59. Taniguchi, M., Sasaki, N., Tsuge, T., Aoyama, T. & Oka, A. ARR1 directly activates cytokinin response genes that encode proteins with diverse regulatory functions. *Plant Cell Physiol.* **48**, 263–277 (2007).
60. Wu, F. H. et al. Tape–*Arabidopsis* sandwich—a simpler *Arabidopsis* protoplast isolation method. *Plant Methods* **5**, 16 (2009).

61. Shimotohno, A., Heidstra, R., Blilou, I. & Scheres, B. Root stem cell niche organizer specification by molecular convergence of PLETHORA and SCARECROW transcription factor modules. *Genes Dev.* **32**, 1085–1100 (2018).
62. Zhang, G. et al. Jasmonate-mediated wound signalling promotes plant regeneration. *Nat. Plants* **5**, 491–497 (2019).
63. Dobin, A. et al. STAR: ultrafast universal RNA-seq aligner. *Bioinformatics* **29**, 15–21 (2013).
64. Love, M. I., Huber, W. & Anders, S. Moderated estimation of fold change and dispersion for RNA-seq data with DESeq2. *Genome Biol.* **15**, 550 (2014).
65. Chen, S., Zhou, Y., Chen, Y. & Gu, J. fastp: an ultra-fast all-in-one FASTQ preprocessor. *Bioinformatics* **34**, i884–i890 (2018).
66. Smith, T., Heger, A. & Sudbery, I. UMI-tools: modeling sequencing errors in unique molecular identifiers to improve quantification accuracy. *Genome Res.* **27**, 491–499 (2017).
67. Stuart, T. et al. Comprehensive integration of single-cell data. *Cell* **177**, 1888–1902.e21 (2019).
68. Haga, N. et al. Mutations in MYB3R1 and MYB3R4 cause pleiotropic developmental defects and preferential down-regulation of multiple G2/M-specific genes in *Arabidopsis*. *Plant Physiol.* **157**, 706–717 (2011).
69. Kobayashi, K. et al. Transcriptional repression by MYB3R proteins regulates plant organ growth. *EMBO J.* **34**, 1992–2007 (2015).
70. Butler, A., Hoffman, P., Smibert, P., Papalexi, E. & Satija, R. Integrating single-cell transcriptomic data across different conditions, technologies, and species. *Nat. Biotechnol.* **36**, 411–420 (2018).
71. Yu, G., Wang, L.-G., Han, Y. & He, Q.-Y. clusterProfiler: an R package for comparing biological themes among gene clusters. *OMICS* **16**, 284–287 (2012).
72. Trapnell, C. et al. The dynamics and regulators of cell fate decisions are revealed by pseudotemporal ordering of single cells. *Nat. Biotechnol.* **32**, 381–386 (2014).

Acknowledgements

We thank ABRC, T. Xu and J.-W. Wang for providing mutant seeds and marker lines. This work was supported by grants from the National Natural Science Foundation of China (no. 31630007), the Strategic Priority Research Program of the Chinese Academy of Sciences (no. XDB27030103), Youth Innovation Promotion Association CAS (no. 2014241) and the National Key Laboratory of Plant Molecular Genetics to L.X.

Author contributions

N.Z. and L.X. designed the research, analysed the data and wrote the article. N.Z. performed the experiments.

Competing interests

The authors declare no competing interests.

Additional information

Supplementary information The online version contains supplementary material available at https://doi.org/10.1038/s41477-021-01015-8.

Correspondence and requests for materials should be addressed to Lin Xu.

Peer review information *Nature Plants* thanks Kalika Prasad, Pil Joon Seo and the other, anonymous, reviewer(s) for their contribution to the peer review of this work.

Reprints and permissions information is available at www.nature.com/reprints.

Publisher's note Springer Nature remains neutral with regard to jurisdictional claims in published maps and institutional affiliations.

nature research

Corresponding author(s): Lin Xu

Last updated by author(s): Sep 8, 2021

Reporting Summary

Nature Research wishes to improve the reproducibility of the work that we publish. This form provides structure for consistency and transparency in reporting. For further information on Nature Research policies, see our Editorial Policies and the Editorial Policy Checklist.

Statistics

For all statistical analyses, confirm that the following items are present in the figure legend, table legend, main text, or Methods section.

n/a	Confirmed
☐	☒ The exact sample size (*n*) for each experimental group/condition, given as a discrete number and unit of measurement
☐	☒ A statement on whether measurements were taken from distinct samples or whether the same sample was measured repeatedly
☐	☒ The statistical test(s) used AND whether they are one- or two-sided *Only common tests should be described solely by name; describe more complex techniques in the Methods section.*
☒	☐ A description of all covariates tested
☒	☐ A description of any assumptions or corrections, such as tests of normality and adjustment for multiple comparisons
☐	☒ A full description of the statistical parameters including central tendency (e.g. means) or other basic estimates (e.g. regression coefficient) AND variation (e.g. standard deviation) or associated estimates of uncertainty (e.g. confidence intervals)
☐	☒ For null hypothesis testing, the test statistic (e.g. *F*, *t*, *r*) with confidence intervals, effect sizes, degrees of freedom and *P* value noted *Give P values as exact values whenever suitable.*
☒	☐ For Bayesian analysis, information on the choice of priors and Markov chain Monte Carlo settings
☒	☐ For hierarchical and complex designs, identification of the appropriate level for tests and full reporting of outcomes
☒	☐ Estimates of effect sizes (e.g. Cohen's *d*, Pearson's *r*), indicating how they were calculated

Our web collection on statistics for biologists contains articles on many of the points above.

Software and code

Policy information about availability of computer code

Data collection	Shoot and root regeneration images were taken by Nikon SMZ1500 Stereoscopic Microscope. Confocal microscopy images were taken by Nikon C2plus. DIC images were taken by Nikon 80i. Luciferase activities were measured by BioTek SYNERGY2. Western blot images were developed and captured by GE ImageQuant LAS4000. qRT-PCR was performed by Biorad CFX96. RNA-seq was performed using the Illumina HiSeq 3000 platform. For single-cell RNA-seq, BD Rhapsody system was used to capture the transcriptomic information of single protoplasts.
Data analysis	Fluorescence quantification was carried out by Nikon C2plus microscope software NIS-Elements AR (version 5.10). Statistical analyses were conducted by R (version 4.0.2). For RNA-seq analysis, mapping of reads to the Arabidopsis thaliana genome (TAIR10) and transcript counting were conducted using STAR (version 2.7.2b). Differentially expressed genes were determined by DESeq2 (version 1.28.1). GO analyses were performed using clusterProfiler (version 3.16.1). For single-cell RNA-seq analysis, we applied fastp (version 0.20.1) with default parameter to filter the adaptor sequence and remove the low quality reads to achieve the clean data. UMI-tools (version 1.0.0) was applied for Single Cell Transcriptome Analysis to identify the cell barcode whitelist. The UMI-based clean data were mapped to Arabidopsis thaliana genome (TAIR10) utilizing STAR (version 2.7.2b) mapping with customized parameter from UMI-tools standard pipeline to obtain the UMIs counts of each sample. Seurat package (version 3.0) was used to analyze scRNA-seq expression matrix. DDRTree from Monocle2 (version 2.18.0) was used to construct pseudotime development trajectory. AUCell (version 1.14.0) was used for analysis of QC identity in callus.

For manuscripts utilizing custom algorithms or software that are central to the research but not yet described in published literature, software must be made available to editors and reviewers. We strongly encourage code deposition in a community repository (e.g. GitHub). See the Nature Research guidelines for submitting code & software for further information.

Data

Policy information about availability of data

All manuscripts must include a data availability statement. This statement should provide the following information, where applicable:

- Accession codes, unique identifiers, or web links for publicly available datasets
- A list of figures that have associated raw data
- A description of any restrictions on data availability

Sequence data can be accessed at the Arabidopsis Genome Initiative under the following accession numbers: WOX11 (AT3G03660), WOX5 (AT3G11260), WOX7 (AT5G05770), PLT1 (AT3G20840), PLT2 (AT1G51190), SCR (AT3G54220), ARR5 (AT3G48100), ARR7 (AT1G19050), ARR12 (AT2G25180), ARR2 (AT4G16110), WUS (AT2G17950), JKD (AT5G03150), TAA1 (AT1G70560), TAR2 (AT4G24670), KCS6 (AT1G68530), PDF1 (AT2G42840), ATML1 (AT4G21750), BDG1 (AT1G64670), PIN2 (AT5G57090), SCZ (AT1G46264), NPY4 (AT2G23050), HAN (AT3G50870), SMXL3 (AT3G52490), TMO5 (AT3G25710), WAT1 (AT1G75500), ANT (AT4G37750), ATHB8 (AT4G32880), 4CL1 (AT1G51680), PXY (AT5G61480), bHLH068 (AT4G29100), TAN1 (AT3G05330), HIK (AT1G18370). The RNA-seq and single-cell RNA-seq data have been deposited in the Gene Expression Omnibus (GEO, http://www.ncbi.nlm.nih.gov/geo) under the accession numbers GSE156990, GSE178354, and GSE156991. The full scan images for Fig. 2b and 3e are provided as Source Data files. The RNA-seq and single-cell RNA-seq data can be accessed using the online tool (http://xulinlab.cemps.ac.cn/) and gene IDs can be used to search for gene expression patterns. The data that support the findings of this study are available from the corresponding author upon request.

Field-specific reporting

Please select the one below that is the best fit for your research. If you are not sure, read the appropriate sections before making your selection.

☒ Life sciences ☐ Behavioural & social sciences ☐ Ecological, evolutionary & environmental sciences

For a reference copy of the document with all sections, see nature.com/documents/nr-reporting-summary-flat.pdf

Life sciences study design

All studies must disclose on these points even when the disclosure is negative.

Sample size	No sample size calculation was performed. Appropriate sample size has been mentioned in the figure legends. Overall, for shoot or root regeneration experiments, more than 24 individual explants were tested. For fluorescence intensity measurement, 10 individual plants were detected. For qRT-PCR experiments, 3 independent biological replicates were tested. For dual-luciferase reporter assay, at least 3 biological repeats were performed. For RNA-seq analysis, 2 biological replicates were analyzed. Sample size of above experiments was determined to meet the feasibility of data collection and was sufficient to generate statistical significance and reproducibility. For single cell RNA-seq analysis, more than 150 calli from 1 independent experiment were used for sequencing. The sample size of single cell RNA-seq was considered based on pilot assays to generate sufficient cells for BD Rhapsody system.
Data exclusions	No data were excluded from the analyses.
Replication	Single cell RNA-seq was performed with one repeat. Other experiments were performed with at least 2 biological repeats as indicated in figure legends and methods. All attempts at replication were successful.
Randomization	For single cell RNA-seq, ~150 calli were randomly selected and dissected to obtain protoplasts. For tissue culture experiments, specific genotypes were randomly arranged into different medium and exposed to similar growth conditions. For RNA-seq and qRT-PCR analysis, the same amount of samples from different biological repeats were collected randomly.
Blinding	Blinding was not applied due to lack of prior knowledge and expectation of the final results.

Reporting for specific materials, systems and methods

We require information from authors about some types of materials, experimental systems and methods used in many studies. Here, indicate whether each material, system or method listed is relevant to your study. If you are not sure if a list item applies to your research, read the appropriate section before selecting a response.

Materials & experimental systems

n/a	Involved in the study
☐	☒ Antibodies
☒	☐ Eukaryotic cell lines
☒	☐ Palaeontology and archaeology
☒	☐ Animals and other organisms
☒	☐ Human research participants
☒	☐ Clinical data
☒	☐ Dual use research of concern

Methods

n/a	Involved in the study
☒	☐ ChIP-seq
☒	☐ Flow cytometry
☒	☐ MRI-based neuroimaging

Antibodies

Antibodies used

Anti-Flag affinity gel (A2220; Sigma) was used for co-IP. Anti-HA antibody (H6533; Sigma) with 1:5000 dilution and anti-Flag antibody (A8592; Sigma) with 1:5000 dilution were used for Western blot.

Validation

The specificity of all commercially obtained antibodies has been validated by the manufacturers (Sigma), please see websites below:
Anti-Flag affinity gel (A2220; Sigma): https://www.sigmaaldrich.cn/CN/zh/product/sigma/a2220?context=product
Anti-HA antibody (H6533; Sigma): https://www.sigmaaldrich.cn/CN/zh/product/sigma/h6533?context=product
Anti-Flag antibody (A8592; Sigma): https://www.sigmaaldrich.cn/CN/zh/product/sigma/a8592?context=product